11th AIAA/CEAS Aeroacoustics Conference (26th AIAA Aeroacoustics Conference)
23 - 25 May 2005, Monterey, California

AIAA 2005-2881

Prediction of Turbulent Inflow and Trailing-Edge Noise for Wind Turbines

Patrick J. Moriarty*
National Renewable Energy Laboratory, Golden, CO, 80401

Gianfranco Guidati†
Alstom Power Technology Center, Baden-Daettwil, Switzerland

and

Paul Migliore‡
Engineering Consultant, Arvada, CO 80007

Two dominant sources of aeroacoustic noise for operating wind turbines are thought to be noise due to the interaction of atmospheric turbulence with the leading edge of the blades and turbulent boundary layer noise from the trailing edges of the blades. This study examines two new models for these noise sources: one is a simplified version of a previously implemented model of turbulent inflow noise and another is a more sophisticated version of a turbulent boundary layer trailing-edge noise model. Comparisons between simplified and sophisticated models are made as well as comparisons to measured data. The previously developed model for inflow turbulence noise is able to predict the differences in sound level between different airfoil shapes with good accuracy. The model is based on the acoustic analogy and unfortunately is also computationally intensive, making it prohibitively expensive for wind turbine design. A simplified version of this model, which is based on a geometrical analysis of the airfoils, is presented. It is based on the observation that the difference in inflow turbulence noise between an airfoil and a flat plate can be described by a straight line, with the only free parameter being the slope of this line. The simplified model relates this slope to the relative thickness of the airfoil at two points along the chord. Results are presented, which show that such a simple model can reproduce the results of the more sophisticated model with good accuracy below a Strouhal number based on chord of approximately 75. A new turbulent boundary layer trailing-edge noise model was also developed. This model is more complex than the currently implemented semi-empirical algoritms and more accurately models the physical processes that create boundary layer noise. The model uses boundary layer parameters to estimate the trailing edge noise on both sides of a given airfoil. The sound pressure levels for four different airfoils are calculated using this new method and compared to experimental data. The results from this method are also compared to the empirical relations of the original model based on the work of Brooks, Pope, and Marcolini. The accuracy of the new method is as good or slightly better than the original empirical algorithms for most cases studied. It is unclear whether the new trailing-edge noise model is sensitive enough to predict noise differences between airfoil shapes, but further refinement may increase its accuracy.

* Senior engineer, National Wind Technology Center, 1617 Cole Blvd., Golden, CO, 80401, AIAA member.
† Scientist, Segelhof 1, 5405 Baden-Daettwil, Switzerland.
‡ Engineering Consultant, 7015 Nile Ct., Arvada, CO 80007, AIAA Member.

Nomenclature

C	=	airfoil chord
c_f	=	friction coefficient
D	=	airfoil span
$D_{rel,x\%}$	=	thickness to chord ratio at x% chord
IT	=	inflow turbulence noise indicator
$\boldsymbol{k}$	=	wave number vector
$k_{1,3}$	=	wave number in the streamwise and spanwise directions
k_e	=	wave number of energy containing eddies
H_k	=	kinematic shape factor
l_m	=	mixing length scale in boundary layer
L_2	=	integral length scale in direction perpendicular to airfoil surface
L_ε	=	dissipation length scale in boundary layer
P	=	wave number spectrum of surface pressure fluctuations
R	=	observer distance
Re	=	Reynolds number
SL	=	slope of ΔSPL curve
U	=	freestream velocity
U_1	=	velocity in boundary layer in streamwise direction
U_c	=	eddy convection velocity
U_o	=	velocity on edge of boundary layer
x_2	=	coordinate perpendicular to airfoil surface
W	=	Coles' wake function
u^*	=	friction velocity
$\overline{u_2^2}$	=	mean square normal velocity fluctuations
$\overline{u_1 u_2}$	=	turbulent shear stress
α	=	angle of attack or incidence angle
α_{0lift}	=	angle of attack at zero lift
α_{eff}	=	effective angle of attack
α_{geo}	=	geometric angle of attack
δ	=	nominal boundary layer thickness
δ^*	=	boundary layer displacement thickness
ΔSPL	=	difference between flat plat and airfoil sound pressure level
Γ	=	gamma function
κ	=	von Kármán constant
ν	=	kinematic viscosity
ν_t	=	turbulent eddy viscosity
ρ_o	=	air density
θ	=	boundary layer momentum thickness
ϕ_{22}	=	von Kármán spectrum
ϕ_m	=	moving axis spectrum
ω	=	radial frequency

I. Introduction

THE acoustic noise radiating from wind turbines continues to be a dominant design driver that must be incorporated into the design process. The tip speed of many wind turbine designs is limited by the amount of noise created by the blades passing through the atmosphere. Unfortunately, this limitation also caps the amount of energy capture for a specific design, which directly affects the cost of energy. To provide manufacturers with better information for designing future turbine configurations, the U.S. Department of Energy's National Renewable Energy Laboratory (NREL) continues developing and maturing a set of design tools that can be used to predict wind turbine noise.

One of these tools is a noise prediction code[1] originally based on the works of Brooks, Pope, and Marcolini (BPM)[2] and Amiet.[3] This code models six different potential noise sources that are superimposed to estimate the

total noise spectrum emitted from a wind turbine rotor. Two of the noise sources modeled are turbulent inflow noise, which results from turbulence in the atmosphere interacting with the leading edge of the blade, and trailing edge noise, which is created by the turbulent boundary layer on the airfoil interacting with the trailing edge of the blade. As the code has matured,[4,5] the empiricism of various models has been reduced and more validation with measured wind tunnel data has led to further accuracy improvements.

In this study, researchers continue developing the noise prediction algorithms by improving both the turbulent inflow noise and turbulent boundary layer trailing-edge noise methods. Researchers modified the turbulent inflow noise model to reduce the amount of computational resources required to predict this type of noise. This was done by reducing the full boundary-element calculation[5] to a simple relation of geometric dimensions for an airfoil. This resulted in considerable time savings without significant loss in accuracy in predicting turbulent inflow noise below a certain frequency. Above this frequency, the accuracy of the simplified model relative to the original decreased dramatically.

A more complex, physically-realistic, turbulent inflow noise model was introduced into the noise prediction code. This method, originally developed by R. Parchen of TNO-TPD[6,7] and known as the TNO model, more accurately models the boundary layer behavior on an airfoil and its effect on the far field noise. The model relies on a boundary layer prediction routine, XFOIL,[8] to obtain the boundary layer properties. The properties are then used to model the surface pressure fluctuations on the airfoil and the resultant far-field noise. Though this new model uses less empiricism than the original relations of Brooks, Pope, and Marcolini, there is still empiricism present in the modeling of boundary layer properties, such as the integral length scale. This empiricism may continue to limit the accuracy of the new method. However, it is shown that the new TNO model is at least as accurate as the methods of Brooks, Pope, and Marcolini and in some cases more accurate.

While these improvements will eventually be incorporated into the full wind turbine noise prediction code, the results of this study are based on two-dimensional airfoils. The predictions from these improved routines are compared to the results from the original code and also to two-dimensional airfoil acoustic measurements made in a wind tunnel as described below.

II. Inflow Turbulence Noise Model

A. Description of model

In previous studies,[4,9,10] the authors developed a prediction model for inflow-turbulence noise. The model does not give absolute values of sound pressure level, but is able to predict the differences in sound pressure level that result from different airfoil geometries. The model is based on an acoustic analogy and on the boundary-element method. In the method, the turbulence in the incoming flow is represented by harmonic gusts of vorticity that are assumed to passively convect along the streamlines of the steady mean flow around the airfoil. In order to simplify the problem, the vorticity is concentrated into thin vortex sheets that coincide with the streamlines.

The boundary-element method allows the computation of mean flow and the interaction of sound waves with the solid airfoil surface. Using this method, it is possible to consider the true airfoil shape, which makes the model useful as a design tool. The model has been shown to predict the difference between different airfoil shapes correctly.[4] And, when used in conjunction with the flat plate noise model of Amiet,[3] researchers were able to predict absolute sound pressure levels accurately, making the model even more useful for design.

Despite its simplicity, the boundary-element method still requires a significant amount of CPU time to predict a sound spectrum (approximately 5 min. per frequency on a 1.7 GHz PC). While this is considerably faster than any Computational AeroAcoustics (CAA) code, it is too slow when used in connection with a wind turbine noise design code, which considers several airfoil sections along the span of a rotating blade.

To reduce this computational overhead, a simplified model was developed based on geometric parameters of six standard wind turbine airfoils and a NACA 0012 (see Figure 1). All six airfoils used in this initial study have camber. In order to isolate the effect of camber from other geometric effects such as airfoil thickness and angle of attack, some calculations were repeated with decambered airfoils (using XFOIL's[8] geometry manipulation functionality).

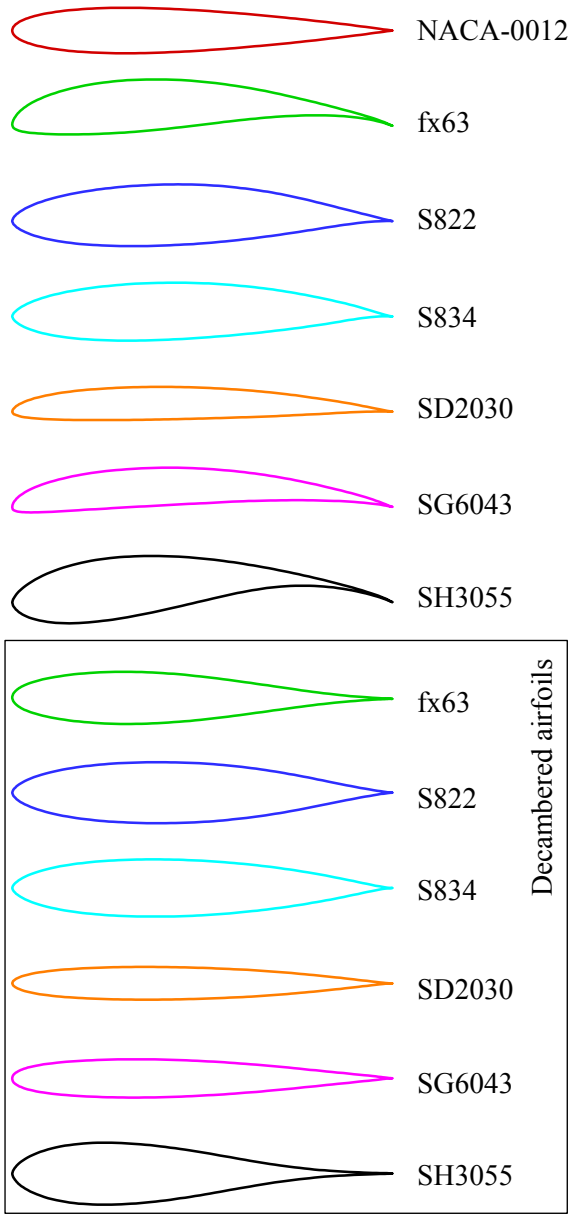

Figure 1. Airfoils used in this study.

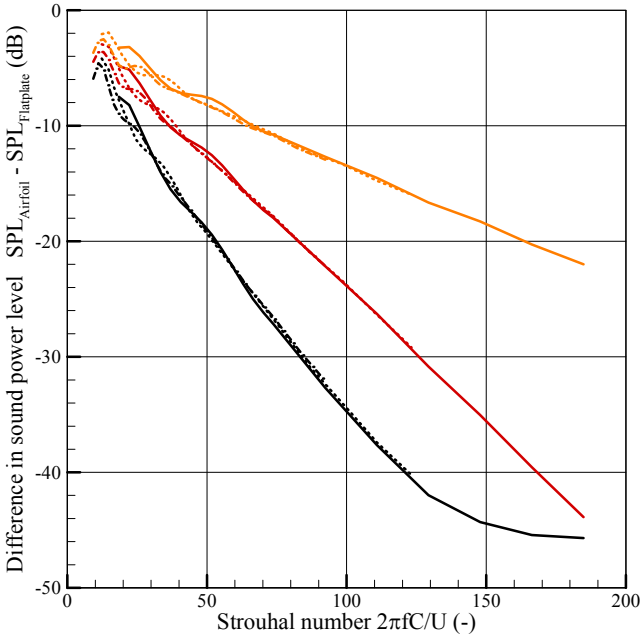

Figure 2. Influence of Mach number on ΔSPL for cambered airfoils (solid – M = 0.1, dashed – M = 0.15, dotted M = 0.2).

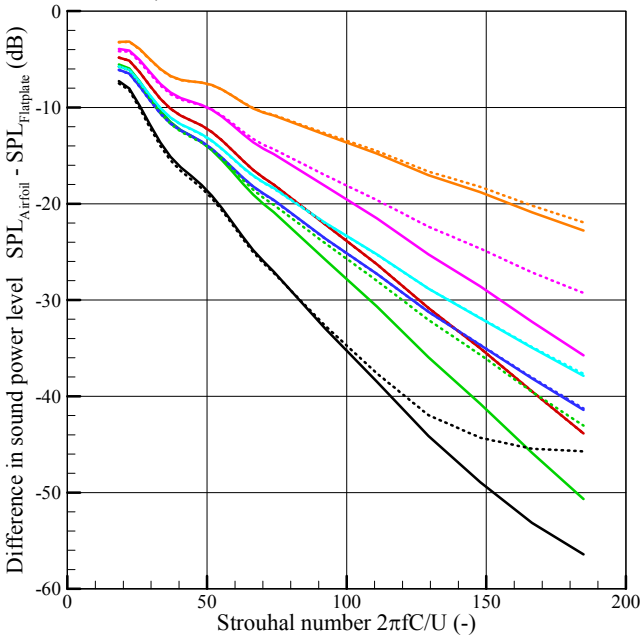

Figure 3. Influence of camber on ΔSPL (solid – uncambered, dotted – cambered).

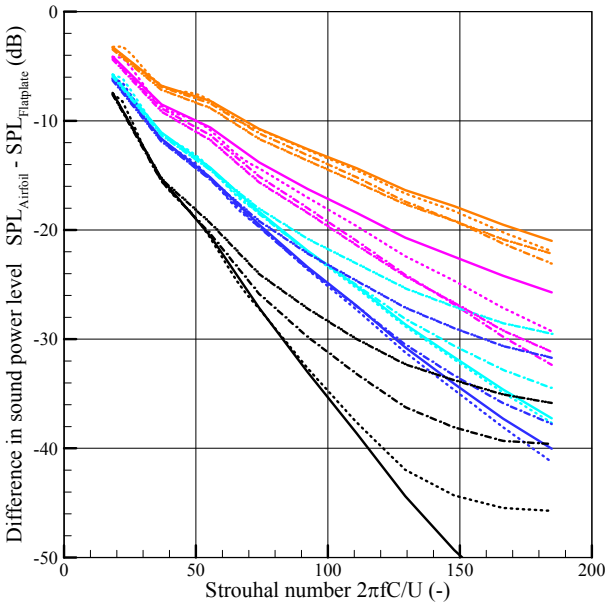

Figure 4. Influence of incidence angle on ΔSPL for cambered airfoils (solid – α = -2°, dotted – α = 0°, dash-dot – α = 2°, dash-dot-dot – α = 4°).

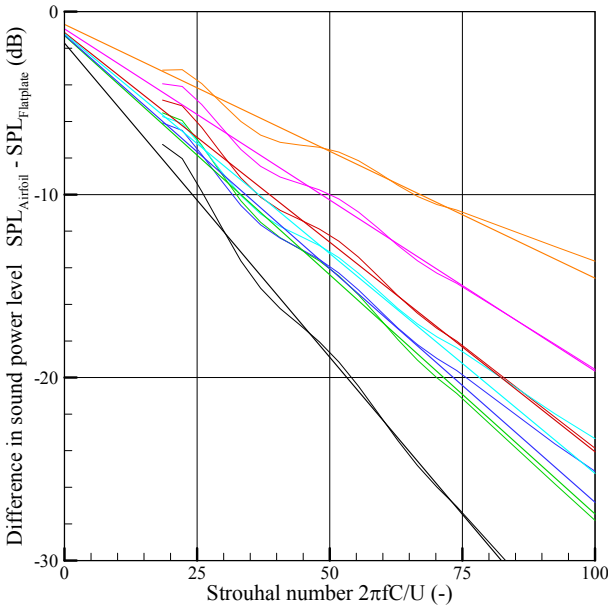

Figure 5. Approximation of ΔSPL curve by straight line for uncambered airfoils at α = 0°.

B. Basis of a simplified model

The authors derived a simplified model of the boundary-element method by observing that the difference between the spectra (ΔSPL) of an airfoil and an infinitely thin flat plate is essentially a line in a diagram which displays ΔSPL vs. a Strouhal number. For a given airfoil this line is independent of Mach number (in the range of interest, M ≈ 0.1-0.2), when plotted vs. Strouhal number based on airfoil chord and freestream velocity (see Figure 2 for selected airfoils). The same plot vs. a Helmholtz number would reveal that the difference between a flat plate and a real airfoil becomes smaller for increasing Mach number. This suggests that the important length scale is a wavelength of the inbound vorticity and not the acoustic wavelength. Figures 3 shows the calculated results for both the cambered and non-cambered airfoils. In this figure, it is obvious that the effect of camber is less important than the thickness distribution of each airfoil. The deviation between the cambered and uncambered results is qualitatively correlated to the amount of camber of the original airfoil, with more highly cambered airfoils having greater deviations at higher Strouhal numbers. This deviation amounts to less than 2 dB below a Strouhal number of 100.

Figure 4 shows the results for the cambered airfoils at different incidence angles (-2 to +4 deg). Again there is a visible influence on the results, but the effect is smaller than the effect of thickness. Below a Strouhal number of approx. 75 the influence of lift and camber on the ΔSPL amounts to less than 2 dB. For a typical Mach number of 0.2 this Strouhal number corresponds to 4 kHz for a 0.2 m airfoil and 800 Hz for 1 m chord length. This can be considered the range of validity of the simplified geometric inflow model presented in the subsequent section.

C. Geometric inflow turbulence model

Figures 2-4 show that the key results of the inflow turbulence noise model, i.e. the difference between a flat plate and an airfoil, can be reduced to a single number, namely the slope *SL* of the ΔSPL curve in a Strouhal plot. Figure 5 shows a linear approximation for the ΔSPL curves of the 7 airfoils. In order to obtain a better fit, a common point for each of these lines was chosen at *St* = –5 and = 0 dB. A simplified inflow turbulence model should be able to predict these slopes based only on the analysis of the airfoil shape, without running the complete boundary-element model. It is known that such a correlation exists in broad terms, namely that airfoils with a 'blunt' leading edge produce less inflow turbulence noise than those with a 'sharp' leading edge. An attempt to derive a more precise description is presented here.

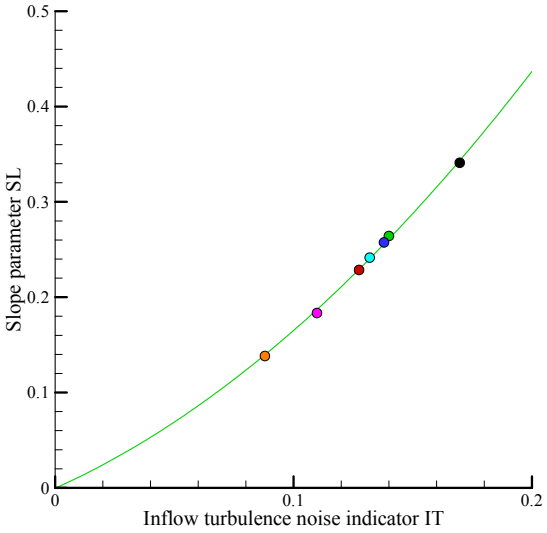

Figure 6. Best fit of *SL* parameter vs. inflow turbulence noise indicator *IT* for airfoils of Figure 1.

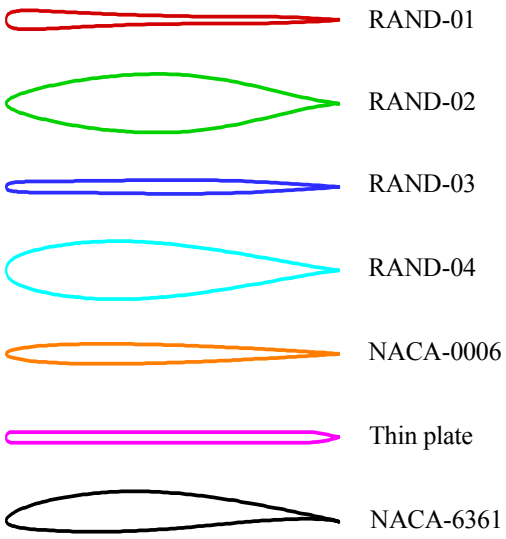

Figure 7. Additional airfoils used for validation.

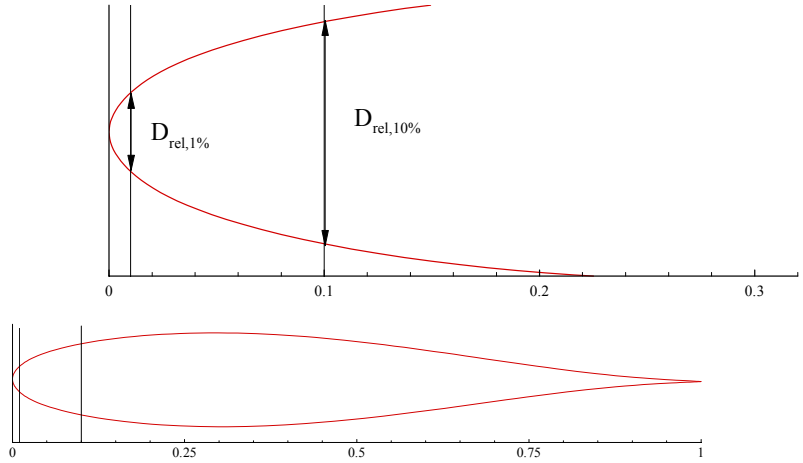

Figure 8. Definition of parameters for inflow turbulence noise indicator *IT*.

The airfoils are analyzed in terms of the following quantities:

- Relative thickness $D_{rel,x\%}$ at x % chord
- Relative thickness $D_{rel,y\%}$ at y % chord

A simple model is proposed for an "inflow turbulence noise indicator" *IT*:

$$IT = D_{rel,x\%} + A \cdot D_{rel,y\%} \,. \tag{1}$$

Each set of free parameters A, x and y leads to a plot of slope parameter *SL* vs. indicator *IT*. A simulated annealing optimization[11] method is used to determine the parameter values that lead to the best quadratic fit of this curve, with the smallest standard deviation between the fit and the calculated values for each airfoil. Here it is assumed that the slope parameter reaches a value of 0 for $IT = 0$, meaning that the airfoil is a flat plate. The results for A, x and y where later rounded in order to obtain practical numbers. Figure 6 shows the best quadratic fit of the slope parameter *SL* versus the indicator *IT*. This was achieved with the following formula for the indicator *IT* (see also Figure 8):

$$IT = D_{rel,1\%} + D_{rel,10\%} \,. \tag{2}$$

The formula for *SL* is given by:

$$SL = 1.123 \cdot IT + 5.317 \cdot IT^2 \,. \tag{3}$$

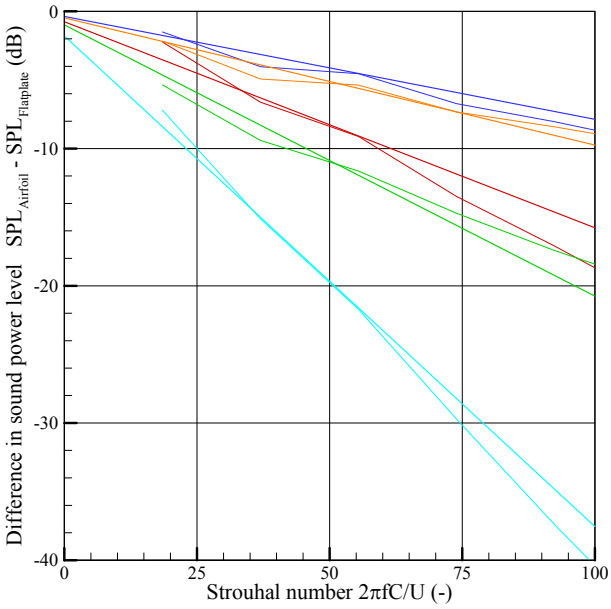

Figure 9. Comparison of ΔSPL curves from complete and simplified inflow turbulence model for additional airfoils (see Figure 7).

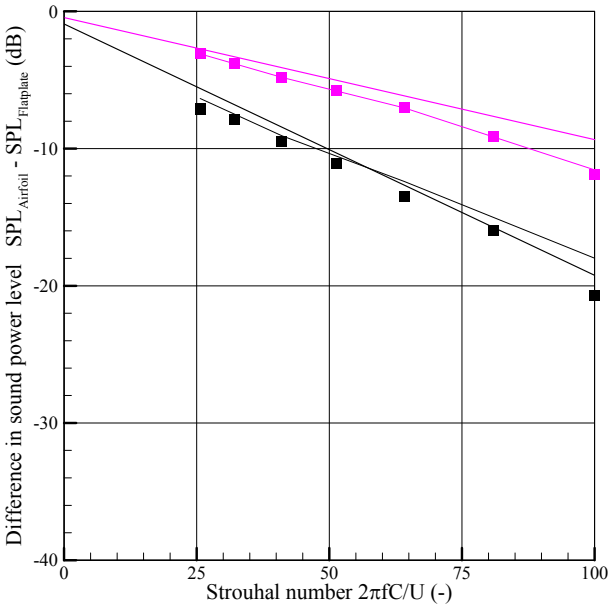

Figure 10. Additional airfoils used for validation.

The complete equation for the difference in sound power level between an airfoil and a flat plate is therefore:

$$\Delta SPL = -\left(1.123\left(D_{rel,1\%} + D_{rel,10\%}\right) + 5.317\left(D_{rel,1\%} + D_{rel,10\%}\right)^2\right)\left(\frac{2\pi fC}{U} + 5\right) \tag{4}$$

Figure 6 proves that this simple model characterizes the behavior of the turbulent inflow noise for 7 airfoils correctly. However, the true value of the model can only be assessed by applying it to other airfoil shapes.

D. Application of geometric inflow turbulence model

The model is tested on 7 additional airfoils, as seen in Figure 7. Four of these belong to a sequence of randomly generated airfoils which exhibit an independent variation of leading edge radius and relative thickness. The others are a NACA-0006, a 3% thick flat plate and a NACA-63612. Calculations were performed both with the full inflow turbulence noise model and the simplified one. As shown in Figure 9, there is a reasonably good agreement between the resulting ΔSPL curves for the first 5 airfoils. Figure 10 shows the thin plate and the NACA-63612 airfoil along with measured data (as symbols).[6] Since a really thin flat plate (i.e. the reference in all plots) was not measured, the measured data for the thin plate are shifted to the levels from the complete inflow turbulence model. The important conclusion from this figure is that the difference between the thin plate and the NACA-63612 is well predicted.

The geometric inflow turbulence noise model can be expressed in a graphical way as shown in Figure 11. The diagram allows construction of ΔSPL curves for several airfoils and a direct estimation of the difference between different airfoil geometries. To use this figure, one needs to (1) determine the relative thickness at 1% and 10% chord, (2) locate the intersection point of the iso-lines for $D_{rel,1\%}$ and $D_{rel,10\%}$, (3) connect the intersection point with the small cross at the top left corner at the x-y point (-5,0) and (4) read the ΔSPL for any Strouhal number. Repeating this for several airfoils allows comparison of relative turbulent inflow noise levels.

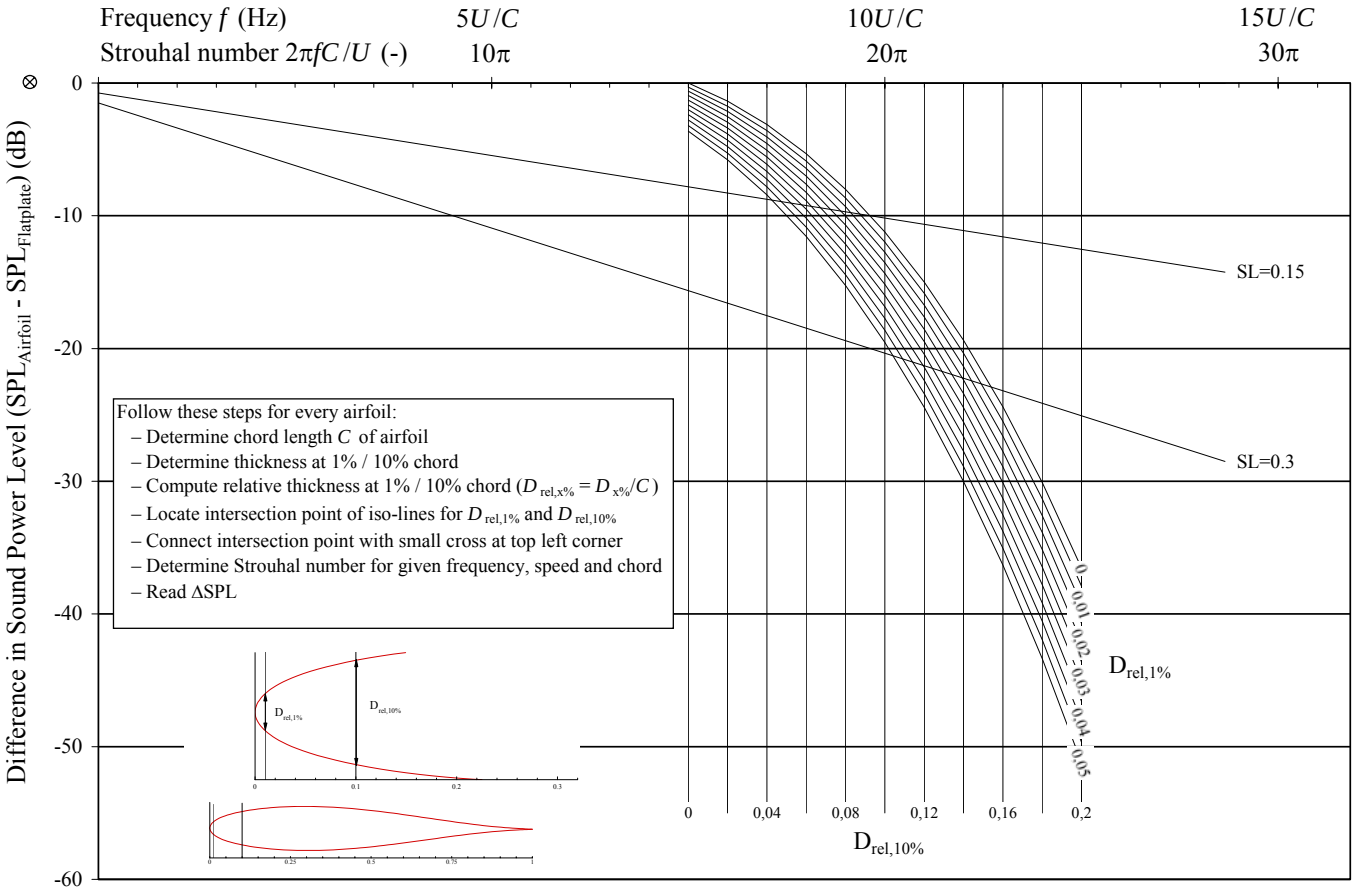

Figure 11. Diagram for the graphical construction of ΔSPL curves for several airfoils.

III. Trailing Edge Noise Model

A. Description of model

In addition to studying a simplified method for modeling the inflow turbulence noise of a wind turbine, we also studied a more sophisticated model for trailing edge noise with more physical detail than the empirical relations of Brooks, Pope, and Marcolini.[1] The new trailing edge noise model was originally developed by Rene Parchen of TNO-TPD in the Netherlands.[6] This approach is based on the work of Blake[12] and uses the wave-number spectrum of unsteady surface pressures to estimate the far field noise. The wave number spectrum is assumed to be a function of the mean velocity gradient, the RMS velocity fluctuations, the integral length scale of the turbulence and a von Kármán spectrum of turbulent fluctuations in the boundary layer on both sides of the airfoil. From this wave number spectrum, the far field noise is calculated assuming that the finite thickness of the trailing edge is negligible and the diffraction is similar to that of an idealized semi-infinite flat plate:

$$S(\omega) = \frac{D}{4\pi R^2}\int_0^\infty \frac{\omega}{c_0 k_1} P(k_1, 0, \omega)\, dk_1 \,. \tag{5}$$

The wave number spectrum $P(k_1, k_3, \omega)$ is a function of several quantities in the boundary layer

$$P(k_1, k_3, \omega) = 4\rho_0^2 \frac{k_1^2}{k_1^2 + k_3^2}\int_0^\infty L_2 \overline{u_2^2}\left(\frac{\partial U_1}{\partial x_2}\right)^2 \phi_{22}(k_1, k_3, \omega)\phi_m(\omega - U_{1,c}k_1)e^{-2|k|x_2} dx_2 \tag{6}$$

All quantities in the above equation need to be modeled as precisely as possible while keeping the model simple. To maintain simplicity, the number of model inputs are limited to three quantities, which are the typical outputs of an integral boundary layer method such as XFOIL:[8] a boundary layer thickness δ, a friction coefficient c_f and the velocity at the edge of the boundary layer U_0. These quantities are extracted at the trailing edge of the airfoil, both at the suction and pressure side. Of these quantities the edge velocity and friction coefficient are direct outputs from XFOIL but the boundary layer thickness needs to be estimated using the relation of Drela and Giles:[14]

$$\delta = \theta\left(3.15 + \frac{1.72}{H_k - 1}\right) + \delta^* . \tag{7}$$

which is based on output quantities of XFOIL, namely the momentum thickness θ, the displacement thickness δ^*, and the kinematic shape factor H_k. The first quantity to be reconstructed is the mean velocity U_1 in the boundary layer. This is achieved by using Coles' law of the wall / law of the wake (see Hinze[14]):

$$U_1 = u^*\left(\frac{1}{\kappa}\ln\left(\frac{u^* x_2}{\nu}\right) + B + \frac{1}{2}W\left(\frac{U_0}{u^*} - \frac{1}{\kappa}\ln\left(\frac{u^*\delta}{\nu}\right) - B\right)\right) \tag{8}$$

with the friction velocity $u^* = U_0\sqrt{c_f/2}$, the two constants, $\kappa = 0.41$ and $B = 5.5$, and the wake function

$$W = 1 - \cos\left(\frac{\pi x_2}{\delta}\right). \tag{9}$$

The next important quantity is the integral length scale L_2 of the turbulence normal to the wall. There are numerous definitions of length scales in turbulent boundary layers. We will use the mixing length l_m and the dissipation length L_ε. Prandtl[14] assumed that the mixing length close to the wall is proportional to the wall distance

$$l_m = \kappa x_2 \qquad \text{for} \qquad x_2 \to 0 \tag{10}$$

Also, it is generally agreed that the mixing length does not increase linearly through the complete boundary (see Figure 7.9 of Townsend[15]). With these constraints in mind, we take the expression of Schlichting[16] who suggested that l_m reaches a maximum of 0.085δ:

$$l_m = 0.085\delta\tanh\left(\frac{\kappa x_2}{0.085\delta}\right). \tag{11}$$

A general formaulation for the dissipation length is

$$L_\varepsilon = \delta\, f\left(\frac{x_2}{\delta}\right). \tag{12}$$

Bradshaw defined a function which peaks at 0.095δ and then drops again towards the outer edge of the boundary layer (see also Figure 7.9 of Townsend). We suggest the following approach

$$L_\varepsilon = c_1\delta x_2\left(1 - e^{-\left(c_2\left(1-\frac{x_2}{\delta}\right)\right)^3}\right), \qquad c_1 \approx 2-4, \;\; c_2 \approx 0.5-1.5 . \tag{13}$$

This ensures a linear behavior at the wall where the length scale increases roughly with the wall distance but allows for some flexibility in the middle and outer part of the boundary layer (see Figure 7.9 of Townsend). We further assume that the integral length scale L_2 equals L_ε.

Prandtl's mixing length hypothesis assumes that the turbulent viscosity ν_t is related to the mixing length by

$$\nu_t = l_m^2\left|\frac{\partial U_1}{\partial x_2}\right|. \tag{14}$$

Consequently, the turbulent shear stress is given by

$$\overline{u_1 u_2} = \nu_t\frac{\partial U_1}{\partial x_2} = l_m^2\left|\frac{\partial U_1}{\partial x_2}\right|\frac{\partial U_1}{\partial x_2} . \tag{15}$$

Townsend gives an overview of ratios between Reynolds stress components (see Table 4.1 in Townsend). A reasonable assumption relating the turbulent shear stress to the normal component is

$$\overline{u_2^2} = \frac{\overline{u_1 u_2}}{c_3} = \frac{1}{c_3} l_m^2 \left|\frac{\partial U_1}{\partial x_2}\right| \frac{\partial U_1}{\partial x_2} \qquad \text{with} \quad c_3 \approx 0.3 - 0.6 \,. \tag{16}$$

The spectrum of normal velocity fluctuations is modeled by a van Kármán spectrum:

$$\phi_{22} = \frac{4}{9\pi k_e^2} \frac{\hat{k}_1^2 + \hat{k}_3^2}{\left(1 + \hat{k}_1^2 + \hat{k}_3^2\right)^{7/3}} \,, \tag{17}$$

with the normalized wave numbers defined as $\hat{k}_{1,3} = k_{1,3} / k_e$ and the wave number of energy containing eddies

$$k_e = \frac{\sqrt{\pi}}{L_2} \frac{\Gamma(5/6)}{\Gamma(1/3)} \approx \frac{0.7468}{L_2} \,. \tag{18}$$

Here Γ is the gamma function. The other spectrum used in the calculation, sometimes called the moving axis spectrum, is a Gaussian distribution

$$\phi_m = \frac{1}{\alpha\sqrt{\pi}} e^{-\left(\frac{\omega - U_c k_1}{\alpha}\right)} \,, \tag{19}$$

where the Gaussian constant α is a function of the eddy convection velocity and turbulent length scale

$$\alpha = 0.05 \frac{U_c}{L_2} \,, \tag{20}$$

and the convection velocity of the eddies is a function of the local boundary layer velocity

$$U_c = c_4 U_1, \qquad c_4 \approx 0.7 - 1.0 \,. \tag{21}$$

One disadvantage of the model for mean velocity in the boundary layer (Eq. 8) is that a negative friction coefficient, which is typical for a separated boundary layer, cannot be considered. In this study, when the friction coefficient became negative, it was reset to a small value of c_f = 0.0001. In the following sections, we compare predictions of the TNO model and the empirical method of Brooks, Pope, and Marcolini to measurements made in the wind tunnel at NLR in the Netherlands.[17,18]

B. Selection of optimum model parameters

The relatively simple TNO model requires tuning of some model parameters. The assumptions on the behavior of turbulent stresses and length scales in boundary layers are backed up by experiments, however, these were usually performed under ideal conditions such as flat plates with zero pressure gradients. The reality of turbulent boundary layers is much more complex. The best fit to the measured data[17,18] was obtained with the following parameters

$$\begin{aligned} c_1 &= 3 \\ c_2 &= 0.9 \\ c_3 &= 0.3 \\ c_4 &= 1.0 \end{aligned} \tag{22}$$

C. Discussion of results

Figures 12-18 show the measured data with the predictions from the TNO model. Four airfoils are shown at an intermediate Reynolds number of $0.5 \cdot 10^6$, and three of them at $1.0 \cdot 10^6$. All figures show a variation of nominal, geometrical incidence angle of 0°, 10° and 18°. Due to the jet deflection in the semi-open-jet wind tunnel arrangement, this nominal incidence angle translates to a smaller effective incidence angle, α_{eff}. The exact value depends on the amount of camber of the airfoil. The formula relating to the effective angle of attack to the geometric angle of attack in the study is

$$\alpha_{eff} = \frac{1}{2.26} \alpha_{geo} + \alpha_{0lift} \left(1 - \frac{1}{2.26}\right) \tag{23}$$

where α_{0lift} is the angle of zero lift for a cambered airfoil. This formula approximates the angle where the lift on the airfoil section in an open jet tunnel is equivalent to that in a closed wind tunnel. Note that this is slightly different than the suggested correction in Ref. 17, but we feel it is more appropriate for highly cambered airfoils of this test.

XFOIL calculations were performed for this effective incidence angle, after which noise levels were calculated using the TNO model and compared to measurement. For many measurement conditions, the trailing edge noise level at the mid-span of the models was contaminated by extraneous noise sources at the edges of the models. In these cases, no reliable determination of a sound level can be given. Therefore, some of the plots contain only a small amount of measured data.

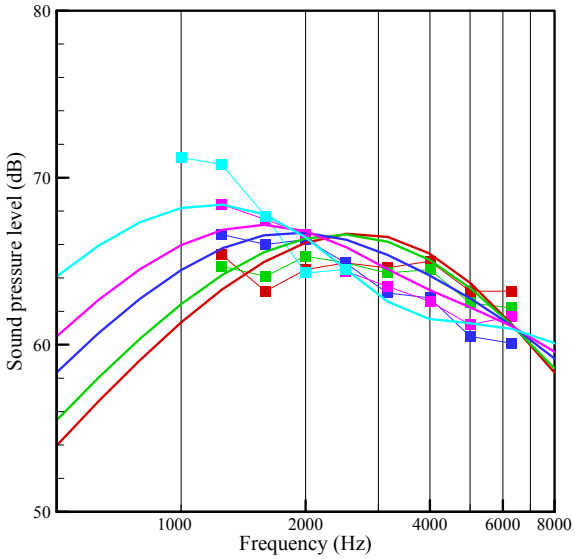

Figure 12. Measured (symbols) and predicted trailing edge noise for NACA 0012, Re = 1.1 · 10^6 at 0°, 4.5°, 9°, 12°, 16.5° geometric incidence angle.

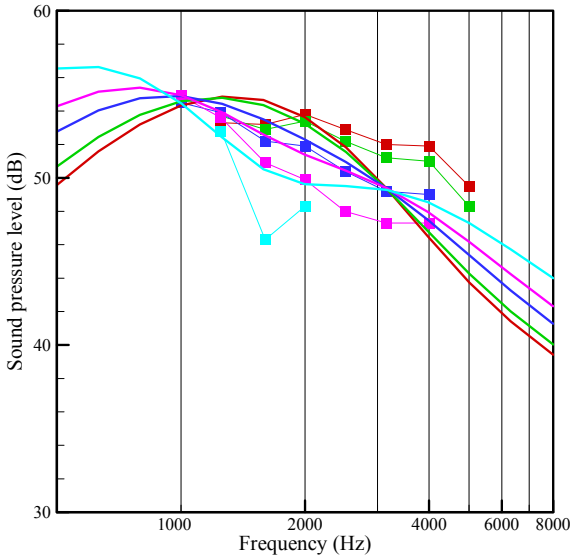

Figure 13. Measured (symbols) and predicted trailing edge noise for NACA 0012, Re = 0.6 · 10^6 at 0°, 4.5°, 9°, 12°, 16.5° geometric incidence angle.

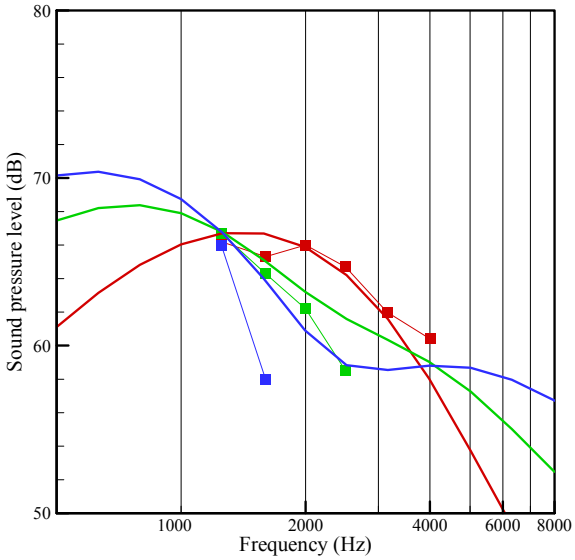

Figure 14. Measured (symbols) and predicted trailing edge noise for S822, Re = 1.0 · 10^6 at 0°, 10°, 18° geometric incidence angle.

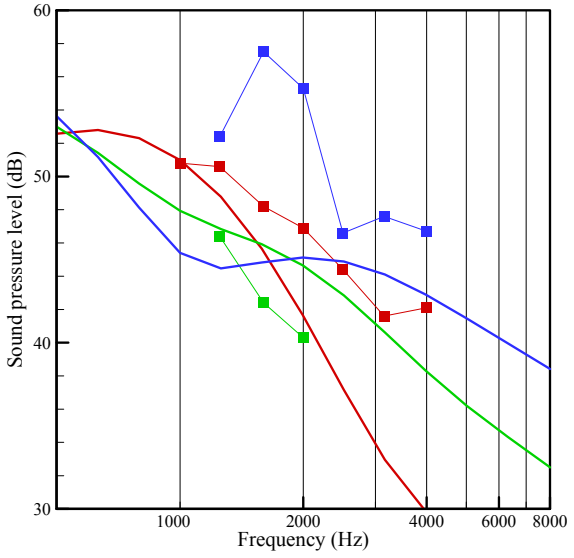

Figure 15. Measured (symbols) and predicted trailing edge noise for S822, Re = 0.5 · 10^6 at 0°, 10°, 18° geometric incidence angle.

In general there is a reasonable agreement between measurements and predictions. Some trends are reproduced correctly: Figure 12 shows the NACA 0012 at a Reynolds number of $1.1 \cdot 10^6$. The measured spectra for the different incidence angles show a clear pattern with an intersection or crossover point at approximately 2.5 kHz. Below this point, the spectra of the higher incidence angles is higher than the spectra for the lower angles. A physical explanation is that the boundary layer at the suction side thickens, which corresponds to larger turbulent eddies and lower frequencies. Above 2.5 kHz the trend is reversed, i.e. the levels at high incidence falls below the levels at low incidence. This broad trend is computed correctly by the model, although the predicted crossover point is closer to 2 kHz. For the same NACA 0012 at $Re = 0.6 \cdot 10^6$ (Figure 13), there is again an intersection point, this time at 1.2 kHz. The part of the spectrum left of this point is not visible due to the insufficient resolution at low frequencies. The predictions show the same intersection, again at a somewhat lower frequency. Although these trends are seen in both predictions and measurements there is clearly a discrepancy in the absolute levels.

For the S822 airfoil (Figures 14, 15), a similar pattern is visible, with an intersection point of the spectra. In the range of valid measurements, the noise level decreases with incidence angle. However, the predictions indicate that this is frequency dependent, since the trend between the incidence angles is reversed at lower frequencies. The spectrum at the highest incidence for the S822 at $Re = 0.5 \cdot 10^6$ seems to be contaminated by a tone, which is not covered by the TNO model. Similar observations can be found for the SH3055 airfoil (Figures 16, 17). Here, the part of the spectrum where the high incidence case dominates is visible in the measurements. The predictions reproduce this trend correctly. Although, the small number of valid data points prohibits any definitive conclusions for the airfoil at the lowest Reynolds number. Finally, the results for the SD2030 airfoil (Figure 18) show qualitative agreement with the measurements, but with some discrepancies in the overall levels.

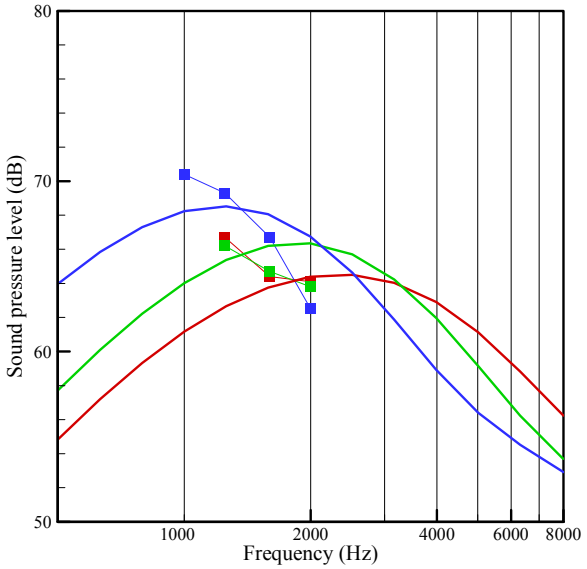

Figure 16. Measured (symbols) and predicted trailing edge noise, SH3055 at Re = $1.0 \cdot 10^6$ at 0°, 10°, 18° geometric incidence angle.

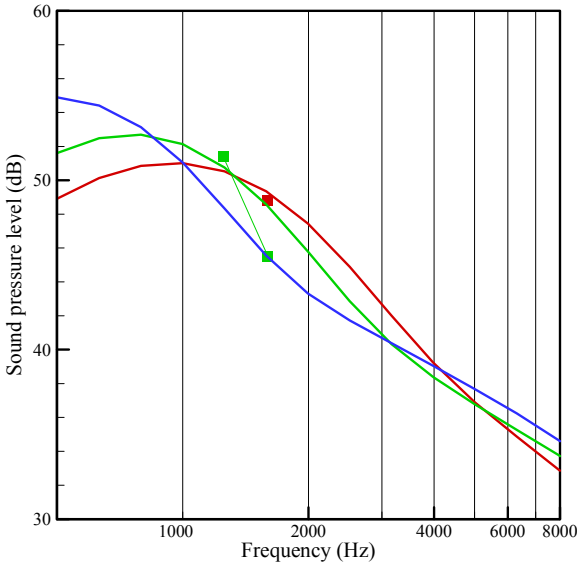

Figure 17. Measured (symbols) and predicted trailing edge noise, SH3055 at Re = $0.5 \cdot 10^6$ at 0°, 10°, 18° geometric incidence angle.

D. Comparison to Brooks, Pope and Marcolini Model

We also repeated the calculations of Figures 12-18 using a slightly modified version Brooks Pope and Marcolini (BPM) model. The model was modified by using the calculated boundary layer thicknesses from XFOIL, instead of the empirical thicknesses in the original BPM model.

One trend that was immediately obvious for all airfoils, was that the separation noise of the BPM model dominated once the angle of attack was greater than about 5°. Because of this, the sound pressure level at all frequencies also increased, as seen in Figure 19. In the measured data, the sound pressure levels do increase with angle of attack at low frequency, but at high frequencies the opposite is true. This results in a crossover frequency where they sound pressure level is fairly independent of the angle. In Figure 19, this frequency is 2.5 kHz. The full BPM model does not correctly model this effect. However, if separation noise is neglected, leaving just the turbulent boundary layer noise from both sides of the airfoil, this phenomenon can be reproduced and there is actually better agreement with the measured data and the sound pressure levels predicted by the TNO model. All further plots in this paper will use this modified version of the BPM model without separation noise.

Figures 20-21 to show the measured data compared to the BPM prediction for a NACA 0012. These data are identical to those in Figures 12 and 13. Comparing the BPM predictions to those of the TNO model, it appears that the TNO model does a better job of predicting the absolute levels, while the BPM tends to overpredict the measured values. Interestingly, the crossover frequency, where the low angle of attack airfoil becomes louder than the airfoil at high incidence angle, is identical between the BPM and TNO for a Reynolds number of $1.1 \cdot 10^6$. At the lower Reynolds number the TNO crossover frequency is lower than that of the BPM model. Also, the BPM model predicts only one such crossover frequency, whereas the TNO predicts two.

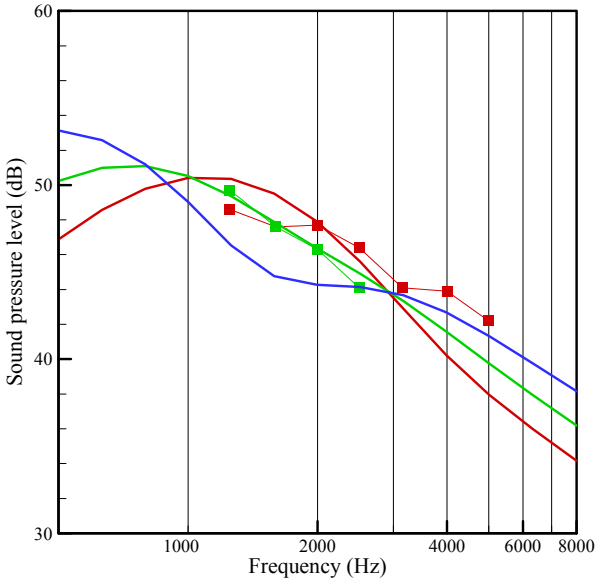

Figure 18. Measured (symbols) and predicted trailing edge noise for SD2030, Re = $0.5 \cdot 10^6$ at 0°, 10°, 18° geometric incidence angle.

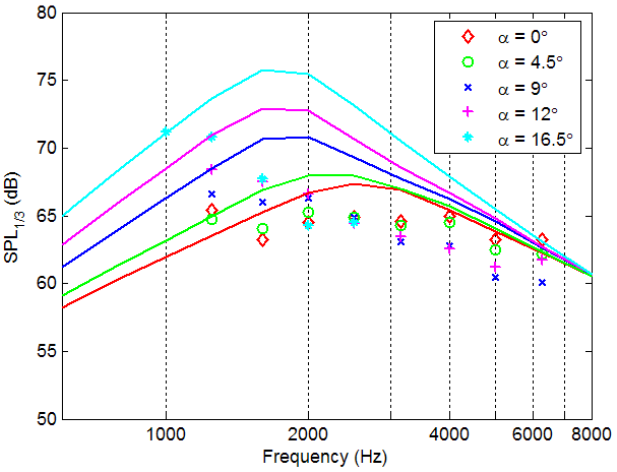

Figure 19. Measured (symbols) and predicted trailing edge noise using the full Brooks, Pope, and Marcolini model or for NACA0012, Re = $1.1 \cdot 10^6$ at 0°, 4.5°, 9°, 12°, 16.5° geometric incidence angle.

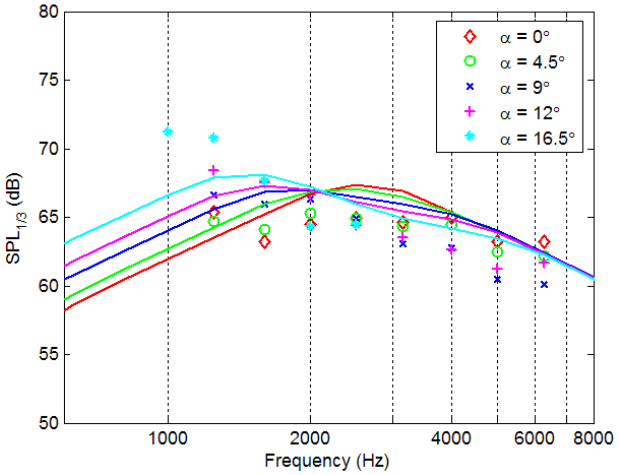

Figure 20. Measured (symbols) and predicted trailing edge noise for NACA0012, Re = $1.1 \cdot 10^6$ at 0°, 4.5°, 9°, 12°, 16.5° geometric incidence angle.

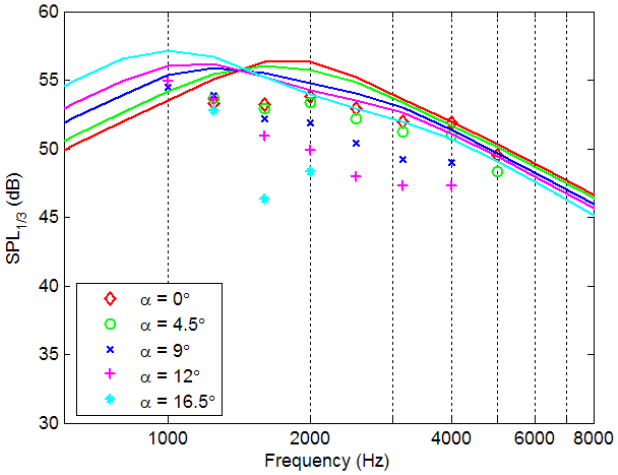

Figure 21. Measured (symbols) and predicted trailing edge noise for NACA0012, Re = $0.6 \cdot 10^6$ at 0°, 4.5°, 9°, 12°, 16.5° geometric incidence angle.

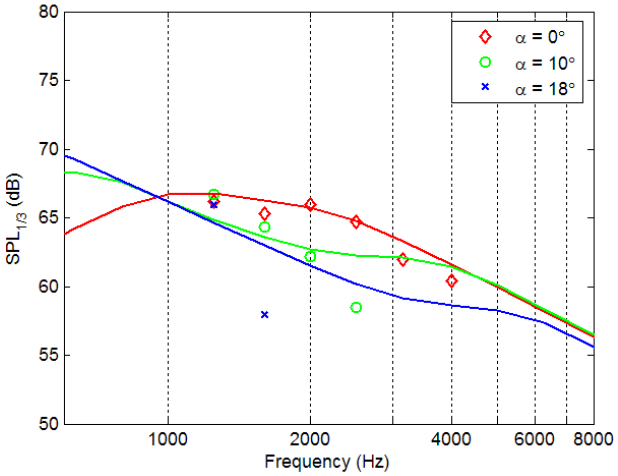

Figure 22. Measured (symbols) and predicted trailing edge noise for S822, Re = $1.0 \cdot 10^6$ at 0°, 10°, 18° geometric incidence angle.

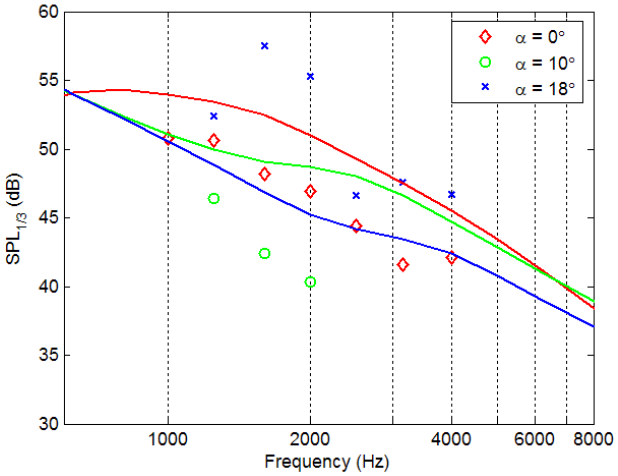

Figure 23. Measured (symbols) and predicted trailing edge noise for S822, Re = $0.5 \cdot 10^6$ at 0°, 10°, 18° geometric incidence angle.

Figures 22 and 23 show predictions for the BPM model of the S822 airfoil along with data that is identical to those shown and Figures 14 and 15. As with the TNO model, the BPM model does a reasonable job of predicting the S822 measurements at a Reynolds number of $1.0 \cdot 10^6$, particularly at the zero incidence angle. The trends are also in good agreement with the measured data in Figure 22. At the lower Reynolds number, however, the agreement is not as good. This is largely because of the previously mentioned tonal peak at the highest incidence angle, which is likely due to laminar vortex shedding noise and not modeled by the TNO method. Comparing these results to those of Figures 14 and 15, it is not obvious whether the TNO or BPM model are more accurate.

Figures 24 and 25 show predicted and the measured sound pressure levels for the SH3055 airfoil. The measured data in these figures are identical to those in Figures 16 and 17. The trends of the predictions seem to compare reasonably with those in the data, although the small number of data points makes it difficult to definitively draw conclusions about the effectiveness of either prediction method for the SH3055 airfoil.

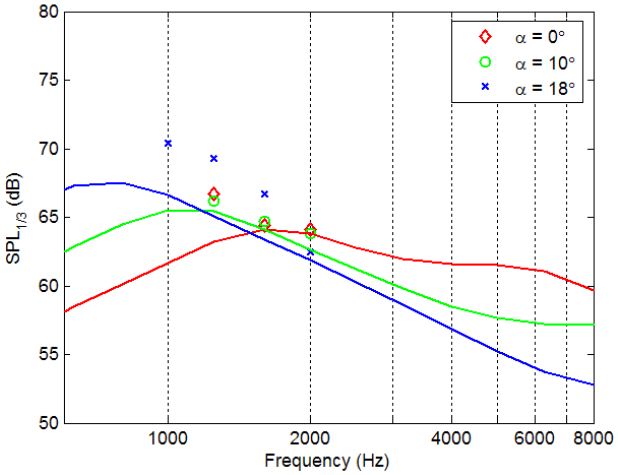

Figure 24. Measured (symbols) and predicted trailing edge noise, SH3055 at Re = 1.0 · 10^6 at 0°, 10°, 18° geometric incidence angle.

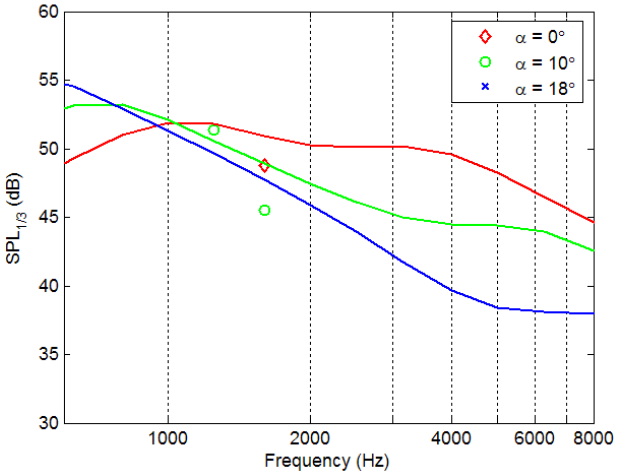

Figure 25. Measured (symbols) and predicted trailing edge noise, SH3055 at Re = 0.5 · 10^6 at 0°, 10°, 18° geometric incidence angle.

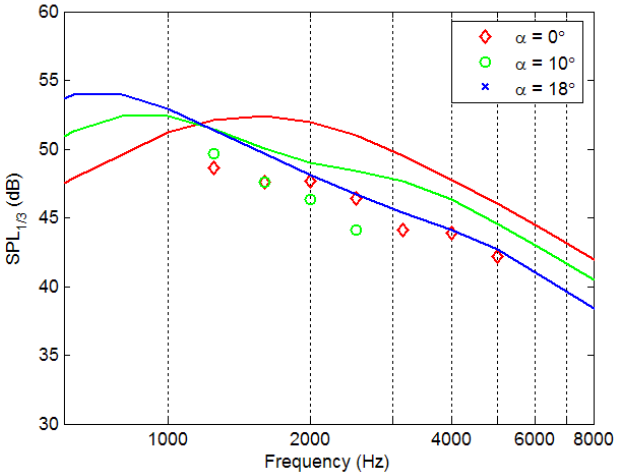

Figure 26. Measured (symbols) and predicted trailing edge noise for SD2030, Re = 0.5 · 10^6 at 0°, 10°, 18° geometric incidence angle.

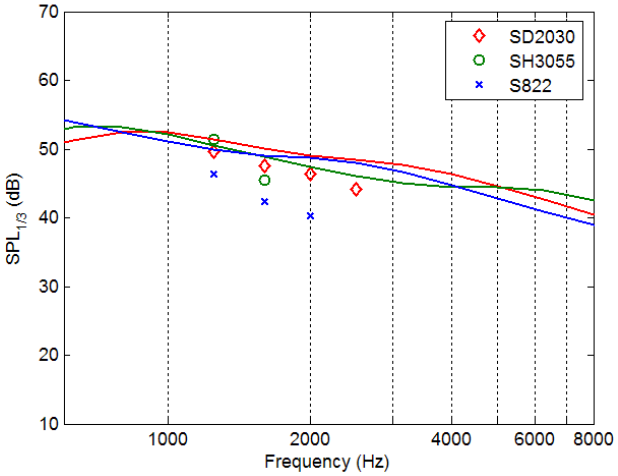

Figure 27. Measured (symbols) and predicted trailing edge noise using BPM model for airfoils at 10° and Re = 0.5 · 10^6 for the SD2030, SH3055, S822 airfoils

Finally, Figure 26 shows the comparison between the BPM model and the measurements for the SD2030 airfoil. For the two lowest angles of attack, the BPM accurately predicts the trends in the data, however the absolute values are overestimated. Comparing these results to Figure 18, it seems that the TNO model is the more accurate prediction for this type of airfoil.

The true test of a prediction method is whether a designer can use it as a tool to design airfoils or choose among a set of airfoils with the lowest noise signatures. From the above comparisons to measured trailing edge noise levels, it is not obvious that either the TNO model or the BPM can differentiate among airfoils under all conditions. For example, Figure 27 is a comparison to measured data of three different airfoils at the same Reynolds number and angle of attack. From the three different sets of measurements, it is obvious that the S822 is the quietest airfoil. But, this is not obvious from the BPM prediction in the figure. Therefore, it would be difficult for a designer using only the BPM prediction method to differentiate between airfoils. The same is true for the TNO model when comparing the results from Figures 15, 17, and 18. The TNO model will predict relatively similar sound pressure level spectra (i.e. 46 dB at 2 kHz for 10° incidence) among airfoils and not reflect the trend in the data. However, it should be noted that in previous studies,[19] researchers were able to design low-noise airfoils using the TNO model whose relative acoustic signatures correlated well with measurements in the wind tunnel at DNW. The reason this correlation is not apparent in the current work requires further research.

IV. Conclusions

This paper presents models for two major aerodynamic noise mechanisms on wind turbine blades. The model for inflow turbulence noise predicts the measured difference in sound spectra between different airfoil shapes with good accuracy, as shown in a previous paper. A simplified version of this model was derived, which relates geometric quantities of an airfoil shape to the sound spectrum. For Strouhal numbers of below 75, the simplified model agrees with the complete model within 2 dB. These results substantiate the rule of thumb that an airfoil with a "blunt" nose produces less inflow turbulence noise than an airfoil with a "sharp" one.

The second noise mechanism modeled is trailing edge noise. A prediction model that uses results from XFOIL, such as the boundary layers thickness and the friction coefficient at the trailing edge, is presented. The model requires several assumptions on the structure of a turbulent boundary layer. The overall predicted levels agree reasonably well with measurements, which were gathered during tests on different airfoils in the NLR acoustic wind tunnel. Certain features of the sound spectra are reproduced, but in other cases the shape of predicted and measured spectra disagree. This noise model also agrees well with results from the empirical model of Brooks, Pope and Marcolini, and in some cases more accurately predicts the measured data. The new method also has the advantage of modeling more of the physical processes that create the noise, which leaves further room for improvement.

A tentative conclusion is that an improved prediction of trailing edge noise will require a more sophisticated calculation of boundary layer properties. For example, the assumptions for the distribution of the integral length scale across the boundary layer are too simplistic. A solution of the full boundary layer equations, instead of an integral boundary layer method, could be an alternative to be studied in the future.

References

[1]Moriarty, P. and Migliore, P., *Semi-Empirical Aeroacoustic Noise Prediction Code for Wind Turbines*, NREL/TP-500-34478, National Renewable Energy Laboratory, Golden, CO, 2003.

[2]Brooks, T., Pope, D., and Marcolini, M., "Airfoil Self-Noise and Prediction," NASA Reference Publication 1218, National Aeronautics and Space Administration, 1989.

[3]Amiet, R., "Acoustic Radiation from an Airfoil in a Turbulent Stream," J. Sound Vibration, Vol. 41, No. 4**,** pp. 407-420, 1975.

[4]Moriarty, P. , Guidati, G., Migliore, P., " Recent Improvement of a Semi-Empirical Aeroacoustic Prediction Code for Wind Turbines," *Proc., 10th AIAA/CEAS Aeroacoustics Conference, Manchester, UK,* AIAA 2004-3041, 2004.

[5]Moriarty, P. "Development and validation of a semi-empirical wind turbine aeroacoustic code," *Proc., 2004 ASME Wind Energy Symposium*, 42nd AIAA Aero. Sci. Mtg., AIAA2004-1189, 2004.

[6]Wagner, S., Guidati, G., Ostertag, J. "Numerical simulation of the aerodynamics and aeroacoustics of horizontal axis wind turbines" *Proceedings of the ECCOMAS 98 conference*, 1998.

[7]Guidati, G., Ostertag J., and Wagner S., "Prediction and reduction of wind turbine noise - An overview of research activities in Europe," *Proc., 2000 ASME Wind Energy Symposium*, 38th AIAA Aero. Sci. Mtg., AIAA2000-0042, 2000.

[8]Drela, M. and Youngren, H.. *XFOIL 6.94 User Guide*, Massachusetts Institute of Technology, Cambridge, Massachusetts, 2001.

[9]Guidati, G., Dassen, T., Parchen, R., Bareiß, R., Wagner, S., "Simulation and Measurement of Inflow-Turbulence Noise on Airfoils," AIAA Paper 97-1698, 1997.

[10]Guidati, G., Wagner, S., "Simulation of Aerodynamic Sound Generation on Airfoils in Low Mach-Number Flows," *Proc., Fifth International Congress on Sound and Vibration*, Adelaide, Australia, 1997.

[11]Press W., Flannery B., Teukolsky S., Vetterling W., *Numerical Recipes in Fortran, 2nd edition*, Cambridge University Press,1992.

[12]Blake W., *Mechanics of Flow-Induced Sound and Vibration, Vol. 1 and 2*, Academic Press Inc., Harcourt Brace Jovanovich, Publishers, 1986.

[13]Drela M. and Giles M., "Viscous-Inviscid Analysis of Transonic and Low Reynolds Number Airfoils," *AIAA Journal*, Vol. 25, No. 10, 1987.

[14]Hinze, J.O., *Turbulence*, McGraw Hill, 1959.

[15]Townsend, A.A., *The structure of turbulent shear flows*, Cambridge University Press, 1976.

[16]Schlichting, H., *Boundary layer theory*, McGraw Hill, 1968.

[17]Oerlemans, S., *Wind Tunnel Aeroacoustic Tests of Six Airfoils for Use on Small Wind Turbines*, National Aerospace Laboratory, Emmeloord, The Netherlands, NREL SR-500-34470, 2003.

[18]Migliore, P.J. and Oerlemans, S., "Wind Tunnel Aeroacoustic Tests of Six Airfoils for Use on Small Wind Turbines," AIAA 2004-1186, to be presented at the 42nd AIAA Aero. Sci. Mtg, 2004.

[19]*Design and Testing of Acoustically Optimized Airfoils for Wind Turbines (DATA), Publishable Final Report*, Non-Nuclear Energy Program, EU Contract JOR3-CT98-0248.